arXiv:1010.6196v1 [cond-mat.soft] 29 Oct 2010

Rotational behavior of red blood cells in suspension—a mesoscale simulation study

By F. Janoschek[1], F. Mancini[2], J. Harting[1,3], and F. Toschi[1,4]

[1] *Department of Applied Physics and J. M. Burgers Centre for Fluid Dynamics, Eindhoven University of Technology, P. O. Box 513, 5600 MB Eindhoven, The Netherlands*

[2] *Department of Physics and INFM, University of Rome "Tor Vergata", Via della Ricerca Scientifica 1, 00133 Rome, Italy*

[3] *Institute for Computational Physics, University of Stuttgart, Pfaffenwaldring 27, 70569 Stuttgart, Germany*

[4] *Department of Mathematics and Computer Science, Eindhoven University of Technology, P. O. Box 513, 5600 MB Eindhoven, The Netherlands*

The nature of blood as a suspension of red blood cells makes computational hemodynamics a demanding task. Our coarse-grained blood model, which builds on a lattice Boltzmann method for soft particle suspensions, enables the study of the collective behavior of the order of 10^6 cells in suspension. After demonstrating the viscosity measurement in Kolmogorov flow, we focus on the statistical analysis of the cell orientation and rotation in Couette flow. We quantify the average inclination with respect to the flow and the nematic order as a function of shear rate and hematocrit. We further record the distribution of rotation periods around the vorticity direction and find a pronounced peak in the vicinity of the theoretical value for free model cells even though cell-cell interactions manifest themselves in a substantial width of the distribution.

Keywords: Coarse-grained hemodynamics, Lattice Boltzmann simulation, Viscosity measurement, Cell orientation, Statistical analysis, Soft particle suspension

1. Introduction

Human blood can be approximated as a suspension of deformable red blood cells (RBCs, also called erythrocytes) in a Newtonian liquid, the blood plasma. The other constituents like leukocytes and thrombocytes can be neglected due to their low volume concentrations. Typical physiological RBC concentrations are around 50 %. In the absence of external stresses, erythrocytes assume the shape of biconcave discs of approximately 8 μm diameter [1]. An understanding of their effect on the rheology and the clotting behavior of blood is necessary for the study of pathological deviations in the body and the design of microfluidic devices for improved blood analysis.

Well-established methods for the computer simulation of blood flow either consist of an elaborate model of deformable cells [2, 3] or restrict themselves to a continuous description at larger scales [4]. Our motivation is to bridge the gap between both classes of models by an intermediate approach: we keep the particulate nature

of blood but simplify the description of each cell as far as possible. The main idea of the model [5] is to distinguish between the long-range hydrodynamic coupling of cells and their complex short-range interactions. Our method is well suited for the implementation of complex boundary conditions and an efficient parallelization on parallel supercomputers. This is important for the accumulation of statistically relevant data to link bulk properties, for example the effective viscosity, to phenomena at the level of single erythrocytes. In this article, we present an alternative method of viscosity measurement and a study of the orientational dynamics of cells in a sheared suspensions. The improved understanding of the dynamic behavior of blood might be used for the optimization of macroscopic simulation methods.

2. Coarse-grained model for blood flow simulations

We apply a D3Q19/BGK lattice Boltzmann method for modeling the blood plasma [6]. The single particle distribution function $n_r(\mathbf{x}, t)$ resembles the fluid traveling with one of $r = 1, \ldots, 19$ discrete velocities $\mathbf{c}_r$ at the three-dimensional lattice position $\mathbf{x}$ and discrete time t. Its evolution in time is determined by the lattice Boltzmann equation

$$n_r(\mathbf{x} + \mathbf{c}_r, t + 1) = n_r(\mathbf{x}, t) - \Omega \quad \text{with} \quad \Omega = \frac{n_r(\mathbf{x}, t) - n_r^{\mathrm{eq}}(\rho(\mathbf{x}, t), \mathbf{u}(\mathbf{x}, t))}{\tau} \tag{2.1}$$

being the BGK-collision term with a single relaxation time τ. The equilibrium distribution function $n_r^{\mathrm{eq}}(\rho, \mathbf{u})$ is an expansion of the Maxwell–Boltzmann distribution. $\rho(\mathbf{x}, t) = \sum_r n_r(\mathbf{x}, t)$ and $\rho(\mathbf{x}, t)\mathbf{u}(\mathbf{x}, t) = \sum_r n_r(\mathbf{x}, t)\mathbf{c}_r$ can be identified as density and momentum. In the limit of small velocities and lattice spacings the Navier–Stokes equations are recovered with a kinematic viscosity of $\nu = (2\tau - 1)/6$, where $\tau = 1$ in this study.

For a coarse-grained description of the hydrodynamic interaction of cells and blood plasma, a method similar to the one by Aidun et al. modeling rigid particles of finite size is applied [7]. It can be seen as a bounce-back boundary condition which is enhanced by a correction term $C = 2\alpha_{c_r}\rho(\mathbf{x} + \mathbf{c}_r, t)\,\mathbf{c}_r\mathbf{v}/c_{\mathrm{s}}^2$ that accounts for a possible local boundary velocity $\mathbf{v}$. The lattice weights α_{c_r} and the speed of sound c_{s} are constants for a given set of discrete velocities. The resulting bounce-back rule

$$n_r(\mathbf{x} + \mathbf{c}_r, t + 1) = n_{\bar{r}}^*(\mathbf{x} + \mathbf{c}_r, t) + C \quad \text{with} \quad n_r^*(\mathbf{x}, t) = n_r(\mathbf{x}, t) - \Omega \tag{2.2}$$

and $\bar{r}$ specifying the direction opposite to r is applied to all fluid distributions that according to Eq. 2.1 would travel along a link that crosses the theoretical cell surface. The momentum $\Delta\mathbf{p}_{\mathrm{fp}} = (2n_{\bar{r}} + C)\,\mathbf{c}_{\bar{r}}$ which is transferred during each time step by each single bounce-back process is used to calculate the resulting force on the boundary.

Instead of the biconcave equilibrium shape of physiological RBCs we choose a simplified ellipsoidal geometry that is defined by two distinct half-axes $R_{\parallel}$ and $R_{\perp}$ parallel and perpendicular to the unit vector $\hat{\mathbf{o}}_i$ which points along the direction of the axis of rotational symmetry of each cell i. Since the resulting volumes are rigid we allow them to overlap in order to account for the deformability of real erythrocytes. We assume a pair of mutual forces $\mathbf{F}_{\mathrm{pp}} = \pm 2n_r^{\mathrm{eq}}(\bar{\rho}, \mathbf{u} = \mathbf{0})\mathbf{c}_r$ at each cell-cell link. This is exactly the momentum transfer during one time step

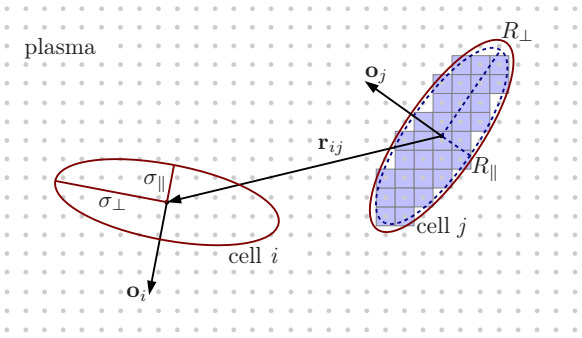

Figure 1. Outline of the model. Shown are two cells with their axes of rotational symmetry depicted by vectors. The volumes defined by the cell-cell interaction are approximately ellipsoidal (—). The smaller ellipsoidal volumes (- - -) of the cell-plasma interaction are discretized on the underlying lattice. (Online version in color.)

due to the rigid-particle algorithm for a resting particle and an adjacent site with resting fluid at equilibrium and initial density $\bar{\rho}$. While these surface forces solely serve to compensate the lack of fluid pressure inside the particles, we additionally implement phenomenological pair potentials for neighboring cells that model the volume exclusion of soft and anisotropic particles in an effective way. For the sake of simplicity, we use the repulsive branch of a Hookian spring potential

$$\phi(r_{ij}) = \begin{cases} \varepsilon \left(1 - r_{ij}/\sigma\right)^2 & r_{ij} < \sigma \\ 0 & r_{ij} \geq \sigma \end{cases} \tag{2.3}$$

for the scalar displacement r_{ij} of two cells i and j. With respect to the disc-shape of RBCs, we follow the approach of Berne and Pechukas [8] and choose the energy and range parameters

$$\varepsilon(\hat{\mathbf{o}}_i, \hat{\mathbf{o}}_j) = \bar{\varepsilon} \left[1 - \chi^2 \left(\hat{\mathbf{o}}_i \hat{\mathbf{o}}_j\right)^2\right]^{-1/2} \tag{2.4}$$

and

$$\sigma(\hat{\mathbf{o}}_i, \hat{\mathbf{o}}_j, \hat{\mathbf{r}}_{ij}) = \bar{\sigma} \left\{1 - \frac{\chi}{2} \left[\frac{\left(\hat{\mathbf{r}}_{ij}\hat{\mathbf{o}}_i + \hat{\mathbf{r}}_{ij}\hat{\mathbf{o}}_j\right)^2}{1 + \chi \hat{\mathbf{o}}_i \hat{\mathbf{o}}_j} + \frac{\left(\hat{\mathbf{r}}_{ij}\hat{\mathbf{o}}_i - \hat{\mathbf{r}}_{ij}\hat{\mathbf{o}}_j\right)^2}{1 - \chi \hat{\mathbf{o}}_i \hat{\mathbf{o}}_j}\right]\right\}^{-1/2} \tag{2.5}$$

as functions of the orientations $\hat{\mathbf{o}}_i$ and $\hat{\mathbf{o}}_j$ of the cells and their normalized center displacement $\hat{\mathbf{r}}_{ij}$. We achieve an anisotropic potential with a zero-energy surface that is approximately that of ellipsoidal discs. Their half-axes parallel $\sigma_\parallel$ and perpendicular $\sigma_\perp$ to the symmetry axis enter Eq. 2.4 and Eq. 2.5 via $\bar{\sigma} = 2\sigma_\perp$ and $\chi = (\sigma_\parallel^2 - \sigma_\perp^2)/(\sigma_\parallel^2 + \sigma_\perp^2)$ whereas $\bar{\varepsilon}$ determines the potential strength.

Fig. 1 shows an outline of the model. Two cells i and j surrounded by blood plasma are displayed. For clarity, the three-dimensional model is visualized in a two-dimensional cut. Depicted are the cell shapes defined by the zero-energy surface of the cell-cell potential Eq. 2.3 with Eq. 2.4 and Eq. 2.5 that can be approximated by ellipsoids with the size parameters $\sigma_\parallel$ and $\sigma_\perp$ as half axes. The cells are free to assume continuous positions and orientations $\mathbf{o}_i$ and $\mathbf{o}_j$. In consequence, also the center displacement vectors $\mathbf{r}_{ij}$ and $\mathbf{r}_{i\mathbf{x}}$ between cells are continuous. Still, for the

cell-plasma interaction an ellipsoidal volume with half axes $R_\parallel$ and $R_\perp$ is discretized on the underlying lattice. For additional clarity, the discretization is drawn only for cell j. The forces and torques emerging from the interaction of the cells with other RBCs and the fluid are integrated by a classical molecular dynamics code in order to evolve the system in time. The conversion from lattice units to physical units is done by multiplication with $\delta x = 2/3\,\mu\text{m}$, $\delta t = 6.80 \times 10^{-8}\,\text{s}$, and $\delta m = 3.05 \times 10^{-16}\,\text{kg}$ for length, time, and mass respectively. As a convention, primed variables are used whenever we refer to quantities specified in physical units. The model parameters are chosen as $R'_\perp = 11/3\,\mu\text{m}$, $R'_\parallel = 11/9\,\mu\text{m}$, $\sigma'_\perp = 4\,\mu\text{m}$, $\sigma'_\parallel = 4/3\,\mu\text{m}$, and $\bar{\varepsilon}' = 1.47 \times 10^{-15}\,\text{J}$. For more detailed information see [5].

3. Results

(*a*) *Apparent bulk viscosity measurement in Kolmogorov flow*

In our previous work, the apparent viscosity of the bulk of the suspension was measured in simulations of unbounded Couette flow [5]. Though this setting is easy to comprise analytically, its efficient and precise implementation proves a non-trivial challenge since the suspended particles would have to be enabled to stretch across the sheared boundary. We therefore demonstrate an alternative method to determine the apparent viscosity that is compatible with completely periodic boundaries and is based on so-called *Kolmogorov flow*: a sinusoidally modulated shear flow. We proceed as in Benzi *et al.* [9] and apply to the full suspension a sinusoidal body force

$$f_z(x) = f_0 \sin\left[k(x - 1/2)\right] \tag{3.1}$$

pointing into the z-direction. f_0 is the amplitude and k the wave number in x-direction. At steady state, the spatial variation of the shear stress

$$\partial_x \sigma_{xz}(x) = f_z(x) \tag{3.2}$$

matches the external forcing. Integration of Eq. 3.2 together with Eq. 3.1 yields an analytic expression for the shear stress

$$\sigma_{xz}(x) = -\frac{f_0}{k} \cos\left[k(x - 1/2)\right] \ . \tag{3.3}$$

The y- and z-averaged local shear rate can be evaluated numerically as

$$\dot{\gamma}_{xz}(x) = \left\langle \partial_x u_z(x) \right\rangle_{y,z} \ . \tag{3.4}$$

After equilibration, a simulation of $N_x \times N_y \times N_z$ lattice sites results in N_x numbers for the apparent viscosity

$$\mu_{\text{app}}(x) = \frac{\sigma_{xz}(x)}{\dot{\gamma}_{xz}(x)} \tag{3.5}$$

covering a range of shear rates that depends on f_0 and k.

Compared to a viscosity measurement in Couette flow [5], the above procedure [9] has the benefit of taking advantage of the whole simulation volume since there are no possibly unphysical boundary regions. Additionally, each single measurement yields data for many different shear rates. On the other side, the non-constant shear stress causes inhomogeneities in the local cell volume concentration

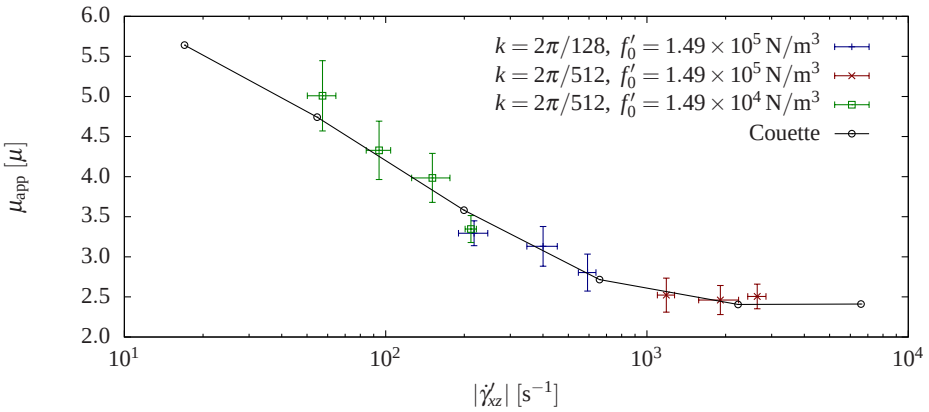

Figure 2. Comparison of viscosity data retrieved from Kolmogorov flow at different wave numbers k and amplitudes of forcing f'_0 after 68.0 ms of equilibration with data measured in Couette flow as in [5]. The hematocrit is $\Phi^* = 43\,\%$ with $\Delta\Phi = 0.5\,\%$ while the error bars were drawn according to the standard deviation after binning and averaging of the original data. (Online version in color.)

$\Phi(x)$ which are much more pronounced than in the case of Couette flow. Therefore, we disregard all viscosity data $(x, \mu_{\mathrm{app}}(x))$ for which $\Phi(x) \notin [\Phi^* - \Delta\Phi, \Phi^* + \Delta\Phi]$ with Φ^* being the volume concentration of interest and $2\Delta\Phi$ a small interval of tolerance. Fig. 2 compares $\mu_{\mathrm{app}}(|\dot{\gamma}_{xz}|)$ resulting from such measurements at varying f_0 and N_x with $k = 2\pi/N_x$ after 68.0 ms with Couette flow measurements as described in [5] ($N_x = 128$). In the plot, $\Phi^* = 43\,\%$ and $\Delta\Phi = 0.5\,\%$. We further average the data within bins with a width of $\Delta[\ln(\dot{\gamma}'_{xz}\,\mathrm{s})] = 0.5$ in order to reduce statistical noise. The good agreement proves the feasibility of the method.

(*b*) *Statistical analysis of cell orientations in Couette flow*

Due to its applicability to huge numbers of particles and the fact that cell orientations are accessible directly in the model, our simulation method is particularly suited for the statistical analysis of RBC orientations at high volume concentrations. In the following, we simulate Couette flow as described in [5]. However, with a size of $N_x = N_z = 512$ and $N_y = 64$ lattice sites, the volume is considerably larger and contains about 3×10^4 cells at a hematocrit of $\Phi = 45\,\%$. The velocity gradient is aligned with x- and the flow with the z-axis. To exclude boundary effects in the x direction, we restrict ourselves to the analysis of those cells which stay at a lateral position $512/3 < x < 2 \times 512/3$ during the whole simulation. The visualization of the cell volumes defined by the model potential is shown for a smaller system in the inset of Fig. 3. It is clear that also at physiological volume concentrations there is a preferential orientation of cells. In order to quantify this observation, the orientation vector of every cell i is multiplied with -1 where necessary to achieve $(\hat{\mathbf{o}}_i)_x > 0$. The angle θ is measured between the positive x-axis and the resulting normalized orientation vector. Fig. 3 displays the most probable value θ^* that is determined by fitting a Gaussian to the distribution of angles. For $\Phi = 45\,\%$, compared to $\theta = 0$ which would mean alignment parallel to the flow, there always is a positive inclination θ^* which is directed against the vorticity of the shear (see inset

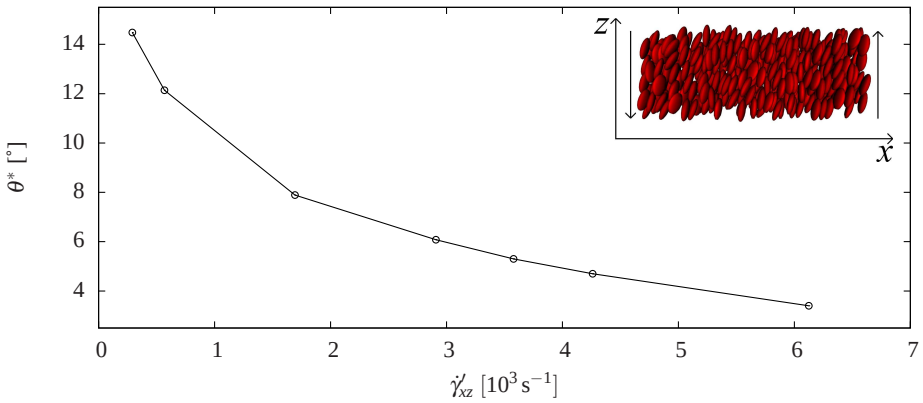

Figure 3. Most probable value of the angle θ between the axis of symmetry of a model cell and the x-direction as a function of the shear rate $|\dot{\gamma}'_{xz}|$ at $\Phi = 45\,\%$. The statistical error of θ is smaller than the symbols. The inset shows alignment of cells due to shear flow in a smaller system. (Online version in color.)

of Fig. 3). When increasing the shear rate from around $300\,\mathrm{s}^{-1}$ to $6000\,\mathrm{s}^{-1}$, this inclination becomes considerably smaller: θ^* decreases from 14.5° to 3.4°.

Studying θ allows to quantify the orientation with respect to the direction of the flow. To quantify the actual amount of orientational order, the nematic order parameter known from liquid crystal physics (see for example [10]) is a better choice. This parameter is usually defined as the largest eigenvalue λ_+ of the nematic order tensor $S_{kl} = \langle 3\hat{o}_k\hat{o}_l - \delta_{kl}\rangle_{i,t}/2$ which is obtained as the average over different time steps t and cells i within the volume of interest. Possible values for λ_+ are comprised between 0 and 1 indicating complete disorder and order. Fig. 4 depicts λ_+ for different shear rates. A decrease of nematic order with increasing shear rate is visible. The inset shows the dependency on the hematocrit Φ at a fixed shear rate of $\dot{\gamma}'_{xz} = (3.0 \pm 0.1) \times 10^3\,\mathrm{s}^{-1}$. For comparison, also λ_+ resulting for a single ellipsoidal particle that tumbles with $\hat{\mathbf{o}}$ perpendicular to the vorticity direction is shown. Apparently, the higher nematic order at $\Phi = 45\,\%$ is caused by hindered tumbling motion while the reason for the lower λ_+ at $\Phi = 11\,\%$ is the lack of alignment in the vorticity plane.

(c) *Statistical analysis of cell rotations in Couette flow*

The above conclusions make clear that preferential orientations result from the averaged tumbling of many cells. The time evolution of the continuous tumbling angle θ is plotted for an arbitrary selection of cells in the inset of Fig. 5. The respective volume concentration is $\Phi = 45\,\%$ and the shear rate $\dot{\gamma}'_{xz} = 6.1 \times 10^3\,\mathrm{s}^{-1}$. The cells keep a largely constant alignment for varying periods of time and, occasionally, flip over by an angle of π along the vorticity direction. Thus, the angular velocity is strongly time-dependent. The probability distribution function of the time required for a rotation by π which is measured as the time T between two flipping events is shown in the main part of Fig. 5. For decreasing volume concentrations, the distribution becomes narrower and its peak is shifted towards shorter times. However, with a width comparable to its average value, even at $\Phi = 11\,\%$ the distribution

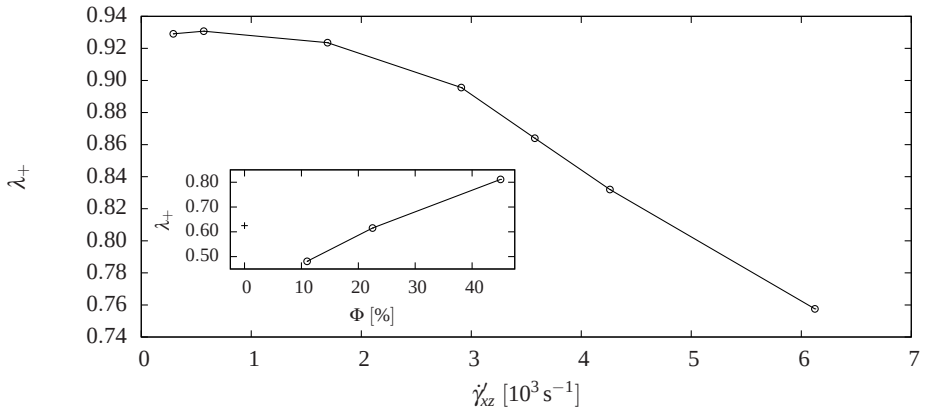

Figure 4. Nematic order parameter λ_+ as a function of the shear rate $\dot{\gamma}'_{xz}$ at $\Phi = 45\,\%$. In the inset, $\dot{\gamma}'_{xz} = (3.0 \pm 0.1) \times 10^3\,\mathrm{s}^{-1}$ is kept fixed and the hematocrit Φ is varied. The single data point at $\Phi \to 0$ is calculated for a single ellipsoidal particle tumbling exactly within the xz-plane [11].

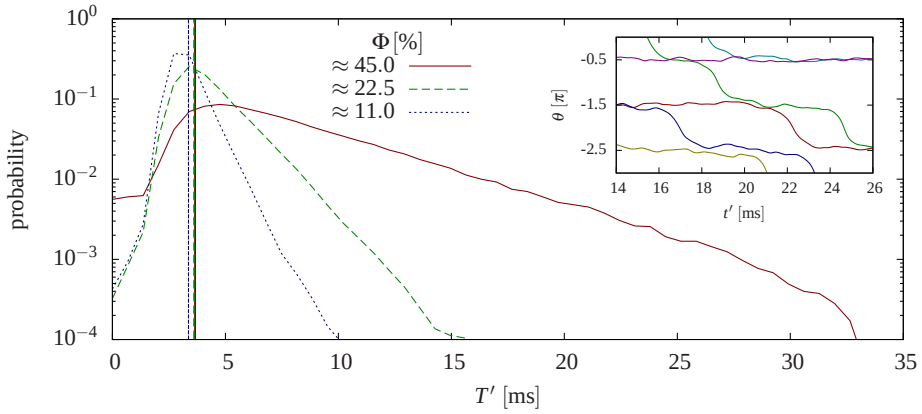

Figure 5. Probability density functions of the time T' between two consecutive events of flipping by an angle of π around the vorticity direction at different values of Φ and $\dot{\gamma}'_{xz} = (3.0 \pm 0.1) \times 10^3\,\mathrm{s}^{-1}$. As a reference, the vertical lines indicate the time required for a rotation around π according to the analytical solution for a single ellipsoidal particle at the respective shear rates [11]. The inset visualizes the continuous tumbling angle θ of selected cells as a function of time t' at $\Phi = 45\,\%$. (Online version in color.)

deviates substantially from a delta peak. Therefore, even though typical tumbling periods in suspension do not differ much from the value for a freely tumbling ellipsoid [11], the effect of cell-cell interactions on our observables is significant for all Φ studied.

4. Conclusion

Our mesoscale model for blood [5] was applied to bulk flow of up to 3×10^4 cells. We demonstrated the feasibility of viscosity measurement in Kolmogorov flow and

studied the statistics of the rotational cell positions and velocities at different values of the hematocrit. These observables are extendable also to more elaborate (e. g. deformable) cell models. Their quantitative study and measurement is a key to build more reliable cell based or continuum descriptions for blood.

The authors acknowledge financial support from the Netherlands Organization for Scientific Research (VIDI grant of J. Harting) and the TU/e High Potential Research Program as well as computing resources from JSC Jülich, SSC Karlsruhe, CSC Espoo, EPCC Edinburgh, and SARA Amsterdam, the latter three being granted by DEISA as part of the DECI-5 project.

References

[1] Fung, Y. C. 1981 *Biomechanics. Mechanical properties of living tissues*. New York: Springer, 1st edn.

[2] Noguchi, H. & Gompper, G. 2005 Shape transitions of fluid vesicles and red blood cells in capillary flows. *PNAS*, **102**, 14 159–14 164. (DOI 10.1073/pnas.0504243102)

[3] Dupin, M. M., Halliday, I., Care, C. M., Alboul, L. & Munn, L. L. 2007 Modeling the flow of dense suspensions of deformable particles in three dimensions. *Phys. Rev. E*, **75**, 066 707. (DOI 10.1103/PhysRevE.75.066707)

[4] Boyd, J., Buick, J. M. & Green, S. 2007 Analysis of the Casson and Carreau-Yasuda non-Newtonian blood models in steady and oscillatory flows using the lattice Boltzmann method. *Phys. Fluids*, **19**, 093 103. (DOI 10.1063/1.2772250)

[5] Janoschek, F., Toschi, F. & Harting, J. 2010 A simplified particulate model for coarse-grained hemodynamics simulations. See http://arxiv.org/abs/1005.2594v2.

[6] Succi, S. 2001 *The lattice Boltzmann equation for fluid dynamics and beyond*. Oxford University Press, 1st edn.

[7] Aidun, C. K., Lu, Y. & Ding, E.-J. 1998 Direct analysis of particulate suspensions with inertia using the discrete Boltzmann equation. *J. Fluid Mech.*, **373**, 287–311.

[8] Berne, B. J. & Pechukas, P. 1972 Gaussian model potentials for molecular interactions. *J. Chem. Phys.*, **56**, 4213–4216. (DOI 10.1063/1.1677837)

[9] Benzi, R., Bernaschi, M., Sbragaglia, M. & Succi, S. 2010 Herschel-Bulkley rheology from lattice kinetic theory of soft-glassy materials. See http://arxiv.org/abs/1004.5058v1.

[10] Tsige, M., Mahajan, M. P., Rosenblatt, C. & Taylor, P. L. 1999 Nematic order in nanoscopic liquid crystal droplets. *Phys. Rev. E*, **60**, 638–644. (DOI 10.1103/PhysRevE.60.638)

[11] Jeffery, G. B. 1922 The motion of ellipsoidal particles immersed in a viscous fluid. *Proc. R. Soc. Lond. A*, **102**, 161–179.